Gold-spiked coating of silver particles through cold nanowelding

Irene Calderon,[a] Ramon A. Alvarez-Puebla,*[a,b] Nicolas Pazos-Perez*[a]

Herein, we present a method to obtain particles composed of a segregated alloy of silver coated with gold. These particles are achieved through the controlled Ostwald ripening of small gold nanoparticles (NPs) onto the surfaces of larger silver particles. The prepared segregated nanoalloyed colloids benefit from the advantages of gold and silver with none of their drawbacks. These platforms provide optical efficiencies which are superior to those of silver with the chemical resistance and biocompatibility of gold.

Introduction

Investigation in gold and silver nanoparticle has been a hot research field during the last forty years. Notably, these two metals present strong localized surface plasmon resonances (LSPRs) when their nanostructures are illuminated in the visible or near infrared (NIR) windows. Consequently, these nanoscaled materials had been used in a variety of applications ranging from spectroscopy,[1] photothermal,[2] drug delivery[3] or hot electron catalysis. [4] Notwithstanding, each material presents its own advantages and drawbacks. For example, gold nanoparticles are easier to produce in controlled size and shape, are chemical resistant and, thus, are highly biocompatible.[5] Conversely, silver nanostructures present a larger excitation window, from the blue to the NIR, as compared with those of gold, from the red to the NIR due to the interband transitions.[6] Also, it can be stated that silver is a much more efficient optical material than gold, giving rise to surface enhanced Raman scattering (SERS) signals over 100-fold higher than similar gold nanostructures due to its larger scattering contribution, associated to the real part of its dielectric function.[7] Therefore, silver nanoparticles are preferred when dealing with *ex vivo* analytical applications,[8] while *in vivo* applications are usually performed using gold colloids.[9]

As an alternative to the use of colloids of a single metal, several approaches had been exercised in the preparation of bimetallic nanoparticles of silver and gold. However, to obtain materials with the advantages of both metals, and none of their drawbacks, a necessary requirement is the formation of a segregated alloy of silver coated with gold. To this end, many synthetic strategies had been designed. The simplest comprise the simultaneous reduction of silver and gold salts.[10] However, this method results in completely uncontrolled materials comprising particles of both metals and their alloys at different concentrations forming solid solutions. Otherwise, the controlled growth of a metal on the surface of preformed colloids yields good results when the metal in the interior (the one forming the colloid) has a larger surface free energy than the metal to be reduced on its surface. Thus, as surface free energy is larger for gold than for silver, 1.128 and 0.923 Jm^{-2}, repectively,[11] segregated alloys of silver are easily grown onto gold colloids.[12] In fact, in many cases, gold is used as a seed to grow silver.[13] The contrary, reduction of gold into silver colloids, results in a solid solution of both metals.[14] A clear example of this can be found in the galvanic replacement reaction using silver colloids and gold salts where the silver of the interior tends to go to the surface while the gold goes to the inner space generating hollow colloidal structures.[15, 16] Another approach has been the use of Ag NPs prepared in aqueous solution that were transferred to organic solvents. In this case, it was reported that as the galvanic replacement reaction proceed and more Au atoms are deposited on the surface, a structure that insulates the Ag core from further oxidative dissolution is formed.[17, 18]

Notably, as a colloid reduces in size, its surface to volume ratio increases. To decrease this energy the system atoms of the surface of the small particle (energetically unfavourable) detach from the particle, as per the Kelvin equation, and diffuse into the solution increasing the concentration of free atoms in solution. When the free atoms are supersaturated, they condense on the surface of larger particles.[19] Thus according to this phenomenon, Ostwald ripening,[20] the larger colloids grow at the expenses of the smaller ones. Ostwald ripening had been extensively employed for the controlled synthesis of gold or silver nanoparticles, [21] hybrid films[22] or thin films at the liquid-gas interface.[23]

Herein, we present a method to obtain particles composed of a segregated alloy of silver coated with gold. These particles are achieved through the controlled Ostwald ripening of small gold nanoparticles onto the surfaces of larger silver particles. The final morphology of the final products depends on reaction times and can be easily controlled by stopping the reaction by separating the exceed of small nanoparticles. Also, these nanoparticles present interesting optical activities which together with their outer morphology can be exploited in both *ex vivo* and *in vivo* applications.

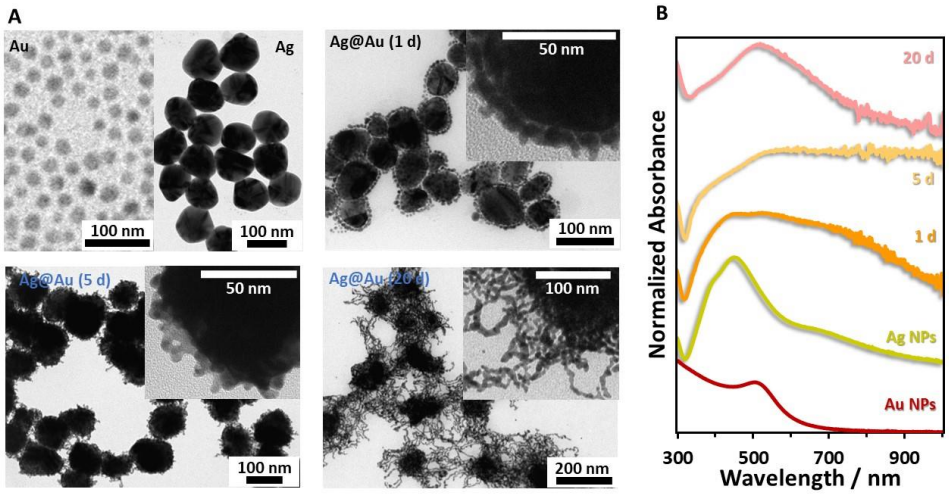

Figure 1. (A) Transmission electron microscopy images of the individual gold seeds and silver nanoparticles (top left) and the segregated alloy of silver coated with gold formed after reaction of the a Ag particles with the Au seeds at different times (1 day top right, 5 days bottom left, and 20 days bottom right). (B) Normalized UV–vis spectra of the corresponding TEM images shown in (A).

Results and discussion

Figure 1A shows transmission electron microscopy (TEM) images of the initial gold and silver particles and their products over the time. As starting materials silver nanoparticles of 90 nm were selected because of their good optical enhancing properties. Conversely, the use of gold nanoseeds was due to their inherent instability due to their small size. Silver nanoparticles, as prepared,[24, 25] present a Zeta potential (ζ) of –42 mV which, considering the analogous negative charge of the, as prepared, gold seeds (ζ = -38 mV), hinder their reaction with other negative entities present in the solution.[26] Thus, to improve the interaction of silver and gold colloids, silver nanospheres were wrapped with branched polyethyleneimine giving rise to particles with a positive charge of 48 mV. The positive silver and negative gold were mixed, and allowed to react, at different particle ratios. Best ratio selected was that of 1:400 for silver and gold particles respectively. Lower ratios improve the reaction kinetics but severely promote the interaction of seeds, between themselves, yielding completely uncontrolled resulting colloids. Conversely, increasing of the particle ratio, increase the reaction time with no clear benefit of the final product control.

After allowing the retention of the gold seeds onto the silver particles under mechanical stirring overnight, the samples were remained in a stirring wheel and aliquots extracted with time. The first extraction after one day of reaction showed silver particles homogeneously coated with the gold nanoseeds, reminiscent of core-satellite structures;[27] However, with time, these segregated alloy of silver coated with gold evolve by a cold nanowelding between the gold and gold and the gold and silver. Composition of the particles was studied with energy dispersive X-ray (EDAX) elemental analysis (Figure 2). This figure shows strong gold signals with reminiscent ones due to silver, suggesting the segregated nature of the formed alloy. Thus, after 5 days a spiked but completely and thin coating of gold on silver can be observed. Larger reaction times increase the gold coating but forming long and refracted shapes rather than compact coatings.

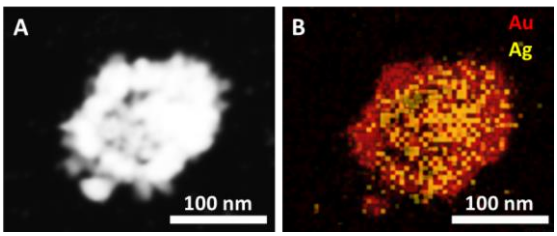

Figure 2. Energy dispersive X-ray elemental analysis of a colloidal particle obtained after 5 days of reaction. (A) SEM image. (B) Mixed elemental mapping (Au in red, Ag in yellow). Clearly showing that the surface of the NP is mainly composed of Au while the inner part is Ag.

Figure 1B shows the localized surface plasmon resonances for these materials. Gold nanoseeds presents the maximum at 520 nm characteristic the dipolar LSPR contribution of these nanoparticles. Silver nanospheres, however, present a complex spectrum due to their size. Rather than just one maximum, three different contributions at 390, 455 and 700, due to the octupole, quadrupole a dipole LSPR.[28] After the addition of the seeds the plasmon shift markedly to the red due, probably, to the formation of electromagnetic hot spots between gold and silver as has been already predicted by theoretical simulations.[29] Notably, after 5 days of reaction, contributions in the red-near infrared gain prominence. The intensification in this optical window can be attributed to the formation of the spikes on the surface, which overlaps ones with other making a continuum signal.[30] After log reaction times (20 days) the particles reshape forming long interconnected gold refracted nanobranches. At this stage the gold contribution almost dominates the LSPR spectrum. As a matter of consideration, it is worthy to note, in the samples prepared with 1 and 5 days of reaction time, the strong contributions bellow 500 nm, characteristic pure silver, that also confirm the segregated nature of the alloy. Figure S1 shows the size distribution and size evolution of the silver NPs and the segregated alloy measured by dynamic light scattering (DLS). These results confirm the progressive increase of the structures during the welding process without any observable aggregation.

As previously stated, the mechanism for the formation of this segregated alloy of silver coated with gold is based in the Ostwald ripening (Figure 3). This process begins with the electrostatic retention of the small seeds on the silver nanoparticle surface. Then, with time the gold nanoseeds weld together and with the silver. As there are many unreacted gold particles in the solution, these free seeds are eventually retained on the surface of the bigger particles, self-assembly to them. The balance between repulsive and attractive forces on seeds makes formation of nanochains particularly favorable.[31] Note that we do not see the strong evidence of epitaxial registry between the NPs known as oriented attachment mechanism.[32, 33] In this case, the surface atoms of the NPs (less stable) which are energetically unfavorable, are in close contact with neighboring particles and therefore, diffuse through the metal surface finding a neighboring atom from the adjacent particle inducing thus, the reshaping and merging of the NPs. As the diffusion barrier for a single metal atom on a metal surface is typically less than 1 eV,[34] room temperature is enough to overcome such a low barrier when the NP are assembled closely together, resulting in the formation of larger plasmonic structures with seed-seed boundaries 'cold welded' together.[35] Similar processes have also been observed for semiconductor nanoparticles.[31] The geometrical evolution of the film with time shows that these structures grow into curved complex geometries, which are metastable. From the perspective of thermodynamics the obvious preference to such asymmetric structures is quite remarkable and can be associated with the asymmetries of the NP surface with low affinity surface ligands.[36] The seed merge proceeds only while are free seeds in solution, with no further changes from this point onwards, due to the decline of NPs in solution and inherent self-limiting mechanisms typical for many nanoparticle assemblies.[37] Thus, centrifugation provides an easy and fast method to quench the reaction and stabilize and nanoparticles. It is important to note, that the presented mechanism also occurs for different core materials than Ag. Figure S2, shows similar evolution of welded Au NPs when SiO_2 was used as core.

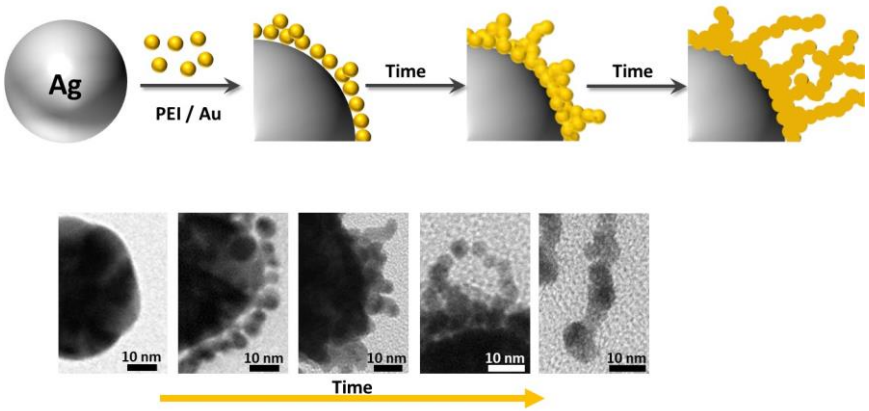

Figure 3. Scheme of the growth mechanism for the segregated alloy of silver coated with gold and TEM images of the different steps.

SERS characterization of the particles produced at different times was characterized with benzenethiol in gas phase and with two laser lines, green (514 nm) and near infrared. Figure 4A shows the SERS spectra with both lasers carried out in the particles reacted during three days. Spectral patterns exhibit the typical band of this molecular probe: 998, 1022 and 10723, ring stretching (ν_{12}), C-H in-plane deformation (ν_{18b}) and C-H in-plane deformation (ν_{18b}).[38, 39] Figure 4B show the comparison of the intensities provided by the ring stretching band (998 cm^{-1}) of isolated colloids on a silicon wafer. This sample was prepared by spin-coating diluted solutions of the colloids on silicon wafers (see Figure 4D-F and Figure S3). For the green laser, the only sample providing SERS was that of segregated alloy of Ag@Au colloids after 1 day of reaction. In this case, the particle is not yet nanowelded and thus, the intergaps between the gold-gold and gold silver particles form electromagnetic hot spots that are capable of enhancing the signal with a single assembled particle. In the case of the rest of samples, either pure metals or their segregated solution, single particles are unable to provide the electric field necessary to yield SERS. Excitation with the 785 nm line neither provide signal for the pure metals, but SERS can be observed in all the alloyed particles. Interestingly, maximum is reached in particles after 5 days of reaction, when a complete shell plus spikes is present in the alloys. These spikes, likely, localize the electromagnetic fields in the apexes of their tips providing the enormous enhancement factors typical of these structures.[40] From this point onwards, the tips grow into branched fibers losing partially the field focalization and consequently the SERS activity. This effect has been already predicted by theoretical simulations and experimentally observed for interacting nanostars.[41, 42] Figure 4C shows the intensity comparison for the same band but in samples prepared by casting of concentrated solutions to generate extended aggregates. In this case, pure silver offers unambiguously better enhancement than whatever of the alloys. This is due to the generation of more efficient hot spots in the near infrared. As silver aggregates, its characteristic LSPR which is in the blue, redshifts to the near infrared providing an excellent substrate for SERS. In the case of the alloys, either does not form efficient interparticle hot spots due to the sterically hindrance provided by the branched gold (such in the cases of samples of 10 and 20 days), or the plasmon, initially placed in the near infrared, shifts to the infrared losing resonance with the excitation light.[43]

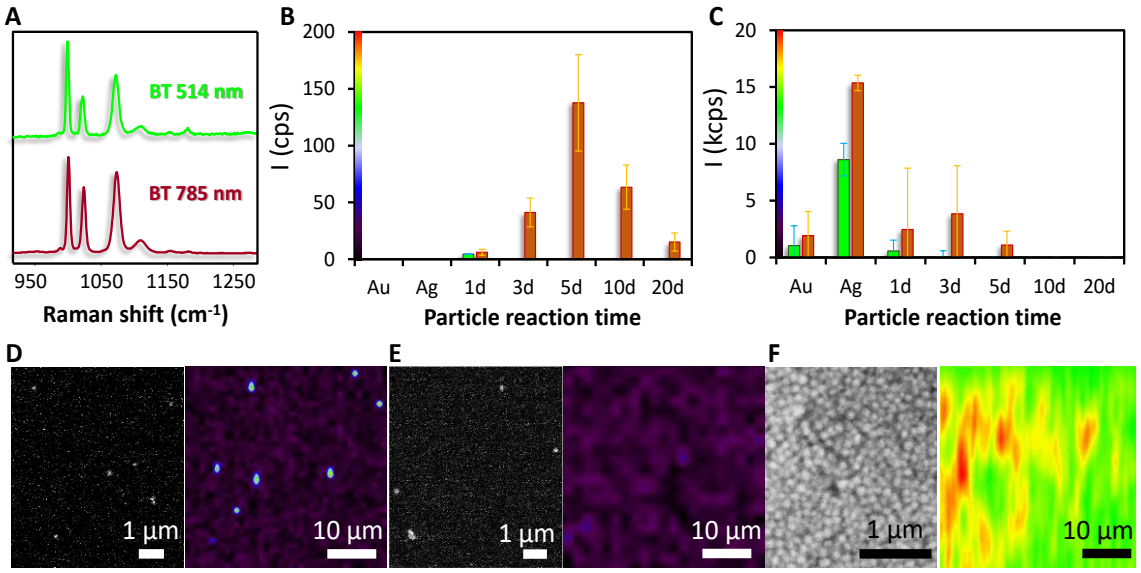

Figure 4. (A) SERS spectra of benzenethiol (BT) on segregated alloy of silver coated with gold with two different lasers, 514 and 785 nm. Comparison of the SERS intensity of the BT ring stretching (998 cm^{-1}) for (B) isolated and (C) aggregates of alloyed particles and the pure metal colloids. (D-F) SEM and SERS images (998 cm^{-1}) examples of the isolated segregated alloy of Ag@Au after 5 days of reaction (D), isolated silver nanoparticles of 90 nm (E) and aggregated silver nanoparticles (F).

Conclusions

In summary we have prepared a collection of segregated alloys of silver coated with gold consisting in silver cores with gold surfaces. This configuration benefits the particles from the advantages of gold and silver with none of their drawbacks. While in aggregated state their optical efficiencies are inferior to those of nanoscaled

pure silver, single particles are capable of single particle SERS, paving the road to the designing of new applications, especially in *in vivo* experiments, where the typical uses of both metals can be simultaneously employed; for example, theragnostic devices for simultaneous detection and treatment. Also, the interesting morphologies of the branched particles suggest an exceptional biocompatibility and internalization in living cells and tissues.

Materials and methods

Materials: Trisodium citrate dihydrated (≥99.5%, $C_6H_5Na_3O_7{\cdot}2H_2O$), ethanol (≥99.9%, EtOH), l-ascorbic acid (≥99.0%, AA), silver nitrate (≥99.9999%, $AgNO_3$), gold(III) chloride trihydrate (≥99.9%, $HAuCl_4{\cdot}3H_2O$), polyethyleneimine branched (≥99.5%, average MW = 25000, PEI), sodium borohydride (99%, $NaBH_4$), and magnesium sulfate (≥ 98%, $MgSO_4$) were purchased from Sigma-Aldrich. All reactants were used without further purification. Milli-Q water (18 MΩ cm^{-1}) was used in all aqueous solutions, and all glassware was cleaned with *aqua regia* before the experiments.

Synthesis of citrate-stabilized spherical silver nanoparticles (ca. 90 nm diameter): Spherical silver nanoparticles of approximately 90 nm diameter were produced by a modification of the kinetically controlled seeded growth method. [24, 25] Briefly, 100 mL of H_2O are heated until boiling under strong magnetic stirring. When it boils energetically, a mixture containing Ascorbic Acid (100 µL, 0.1 M) and Sodium Citrate (1.364 mL, 0.1 M) is added. 1 minute after, a mixture containing $AgNO_3$ (297.6 µL, 0.1 M) and $MgSO_4$ (223.6 µL, 0.1 M) is also added (the $AgNO_3$-$MgSO_4$ mixture was previously incubated for 5 minutes). Boiling and stirring were continued during 1 h. The size of the obtained nanoparticles was around 60 nm. In order to obtain bigger NPs, further growing steps were performed on the produced NPs as follow. One hour after the synthesis, the reaction was cooled until the temperature of the solution reached 90 ºC. Then, a mixture containing Ascorbic Acid (18.2 µL, 0.1 M) and Sodium Citrate (248 µL, 0.1 M) was added, after 2 minutes, 297.6 µL of $AgNO_3$ (0.1 M) were injected under vigorous stirring and the synthesis was left reacting for 30 minutes. This overgrowing process was repeated twice until achieving a NPs size of 87.7 nm. The concentration of the NPs was calculated to be ~ $2.27{\cdot}10^{10}$ NPs/mL by the Lambert–Beer law using an extinction coefficient for silver nanoparticles of 1.3×10^{11} M^{-1} cm^{-1}, derived from the literature.[44] To clean the NPs in order to remove the excess of Sodium Citrate the solution was centrifuged (4.200 rpm, 8 minutes) and further redispersed in MilliQ water to achieve [Ag^0] concentration of $5x10^{-4}$ M.

Ag NPs PEI wrapping: To provide the Ag NPs with positive charge, they were wrapped with a polyelectrolyte monolayer. To this end, 2 mL of the colloidal solution were added drop by drop to a solution of PEI (2 mL, 2 g/L, previously sonicated for 30 min) under vigorous stirring. The sample was incubated for 1 hour. After that PEI was cleaned 5 times by centrifugation at 4000rpm for 5 minutes. The thickness of the PEI layer on the surface of the NPs has been estimated to be around 1.5 to 2 nm.[27]

Synthesis of citrate-stabilized spherical gold nanoparticles with $NaBH_4$ (ca. 5 nm diameter): Briefly, 5 mL of Mili-Q water were mixed with 12,75µL of trisodium citrate (0,1M) and 10,25µL of $HAuCl_4$ (0,12 M) followed by stirring for 10 min at room temperature. Next, 150 µL of a freshly prepared $NaBH_4$ (0.1M) solution was added quickly under vigorous stirring. After 2 min, the stirring rate was reduced, and the seeds were aged for 60 min under slow stirring at room temperature to ensure complete decomposition of $NaBH_4$. The concentration of Au was calculated to be ~$2.5\ 10^{-4}$ M by the amount of Au precursor used giving a concentration of NPs of ~$3.9{\cdot}10^{13}$ NPs/mL.

Formation of Ag coated Au nanoparticles: 2 mL of the PEI wrapped 90 nm Ag NPs ([Ag]= $5{\times}10^{-4}$ M, ~$1.45\ 10^{10}$ NPs/mL) were added drop by drop, under vortex agitation to 0.7 mL of a solution of 5 nm Au nanoparticles (1.25×10^{-4} M, ~$2\ 10^{13}$ NPs/mL). The stoichiometric ratio of Ag:Au NPs was 1:400. The used atomic ratio between Ag:Au was 11.5. To ensure an isotropic 3D coverage of the Ag NPs the solutions was left stirring for 12 hours. Finally, aliquots at different times (1, 3, 5, 10 and 20 days), were collected, centrifuged (4000 rpm, 8 min) and redispersed in the same volume of a 0.25 mM trisodium citrate aqueous solution to stop the branched evolution of the structures.

Synthesis of SiO_2 nanoparticles (ca. 150 nm diameter): Spherical silica nanoparticles of approximately 150 nm diameter were produced by a modification of the Stöber method.[45, 46] By mixing 0.18 mL of H_2O, 8.7 mL EtOH,

625 µL TEOS, and 467 µL NH_4OH. After 12 h, the NPs were cleaned by centrifugation (2 x 9000 rpm, 10 min) and redispersed in 7 mL EtOH. To avoid the dissolution of the NPs in aqueous media, a hardening process was performed by adding 500 µL TEOS (10% in EtOH) to the solution and heating it at 60 °C for 12 h. Next, the NPs were cleaned by centrifugation (2 x 9000 rpm, 10 min) redispersed in 7 mL EtOH to finally transfer them to H_2O (5 mL) by two centrifugation steps (9000 rpm, 10 min).

SiO_2 NPs PEI wrapping: To provide the SiO_2 NPs with positive charge, they were wrapped with a polyelectrolyte monolayer. To this end, 5 mL of the colloidal solution were added drop by drop to a solution of PEI (5 mL, 2 g/L, previously sonicated for 30 min) under vigorous stirring. The sample was incubated for 1 hour. After that PEI was cleaned 5 times by centrifugation at 9000rpm for 10 minutes.

Formation of SiO_2 coated Au nanoparticles: 2 mL of the PEI wrapped 150 nm SiO_2 NPs were added drop by drop, under vortex agitation to 5 mL of a solution of 5 nm Au nanoparticles and the solutions was left stirring for 12 hours. Finally, aliquots at different times (1, and 5 days), were collected, centrifuged (7000 rpm, 8 min) and redispersed in the same volume of a 0.25 mM trisodium citrate aqueous solution to stop the branched evolution of the structures.

Characterization: UV–vis-NIR spectra were recorded using a Thermo Scientific Evolution 201 UV–vis spectrophotometer. Silver concentration for Ag NPs was calculated by the Lambert−Beer law using an extinction coefficient of 6.61×10^{10} M^{-1} cm^{-1}. Zeta potential and DLS size distribution were recorded with a Zetasizer Pro (Malvern) previous dilution of the samples to 1:10 with Milli-Q water. Electron micrographs were recorded with a transmission electron microscopy (JEOL JEM-1011 operating at 80 kV) and an environmental scanning electron microscopy (JEOL 6400) for the structural characterization of the samples and their distribution on the silicon wafers. EDX elemental analysis of the structures was achieved with a FIB-FESEM (Themo Fisher Scios 2).

Substrate deposition of core-satellite assemblies and SERS characterization: Silicon wafers (1cm × 1cm) were cleaned by the standard RCA-1 to remove any possible organic residue. Solutions of all type of NPs structures and their independent building blocks were prepared and 50 µL of each solution were spin coated ((1st ramp) 500 rpm, 10 s; (2nd ramp) 3000 rpm, 30 s with an acceleration rate for both ramps of 500 rpm/s) on the silicon wafers to achieve particle densities ranging of approx. 0.1 to 2 particles × μm^{-2}. SERS spectra were collected in backscattering geometry with a Renishaw Invia Reflex system equipped with a 2D-CCD detector and a Leica confocal microscope. Excitation of the sample was carried out with either 514 or 785 nm laser lines with acquisition times ranging from 1 to 10s and power at the sample of about 0.15 and 3 mW. The laser was focused onto the sample with a x50 objective providing a spatial resolution of ca. 1 µm. SERS maps were obtained in the same conditions in an area of 21 x 21 µm.

Conflicts of interest

There are no conflicts to declare.

Acknowledgements

This work was funded by the Spanish Ministerio de Economia y Competitividad (CTQ2017-88648R and RYC-2015-19107), the Generalitat de Cataluña (2017SGR883) and the Universitat Rovira i Virgili (FR 2019-B2).

Notes and references

1. J. Langer, D. Jimenez de Aberasturi, J. Aizpurua, R. A. Alvarez-Puebla, B. Auguié, J. J. Baumberg, G. C. Bazan, S. E. J. Bell, A. Boisen, A. G. Brolo, J. Choo, D. Cialla-May, V. Deckert, L. Fabris, K. Faulds, F. J. García de Abajo, R. Goodacre, D. Graham, A. J. Haes, C. L. Haynes, C. Huck, T. Itoh, M. Käll, J. Kneipp, N. A. Kotov, H. Kuang, E. C. Le Ru, H. K. Lee, J.-F. Li, X. Y. Ling, S. A. Maier, T. Mayerhöfer, M. Moskovits, K. Murakoshi, J.-M. Nam, S. Nie, Y. Ozaki, I. Pastoriza-Santos, J. Perez-Juste, J. Popp, A. Pucci, S. Reich, B. Ren, G. C. Schatz, T. Shegai, S. Schlücker, L.-L. Tay, K. G. Thomas, Z.-Q. Tian, R. P. Van Duyne, T. Vo-Dinh, Y. Wang, K. A. Willets, C. Xu, H. Xu, Y. Xu, Y. S. Yamamoto, B. Zhao and L. M. Liz-Marzán, *ACS Nano*, 2020, **14**, 28-117.

2. B. Pelaz, C. Alexiou, R. A. Alvarez-Puebla, F. Alves, A. M. Andrews, S. Ashraf, L. P. Balogh, L. Ballerini, A. Bestetti, C. Brendel, S. Bosi, M. Carril, W. C. W. Chan, C. Chen, X. Chen, X. Chen, Z. Cheng, D. Cui, J. Du, C. Dullin, A. Escudero, N. Feliu, M. Gao, M. George, Y. Gogotsi, A. Grünweller, Z. Gu, N. J. Halas, N. Hampp, R. K. Hartmann, M. C. Hersam, P. Hunziker, J. Jian, X. Jiang, P. Jungebluth, P. Kadhiresan, K. Kataoka, A. Khademhosseini, J. Kopeček, N. A. Kotov, H. F. Krug, D. S. Lee, C.-M. Lehr, K. W. Leong, X.-J. Liang, M. Ling Lim, L. M. Liz-Marzán, X. Ma, P. Macchiarini, H. Meng, H. Möhwald, P. Mulvaney, A. E. Nel, S. Nie, P. Nordlander, T. Okano, J. Oliveira, T. H. Park, R. M. Penner, M. Prato, V. Puntes, V. M. Rotello, A. Samarakoon, R. E. Schaak, Y. Shen, S. Sjöqvist, A. G. Skirtach, M. G. Soliman, M. M. Stevens, H.-W. Sung, B. Z. Tang, R. Tietze, B. N. Udugama, J. S. VanEpps, T. Weil, P. S. Weiss, I. Willner, Y. Wu, L. Yang, Z. Yue, Q. Zhang, Q. Zhang, X.-E. Zhang, Y. Zhao, X. Zhou and W. J. Parak, *ACS Nano*, 2017, **11**, 2313-2381.
3. P. Ghosh, G. Han, M. De, C. K. Kim and V. M. Rotello, *Adv. Drug Delivery Rev.* , 2008, **60**, 1307-1315.
4. J. J. Baumberg, *Faraday Discuss.*, 2019, **214**, 501-511.
5. C. J. Murphy, A. M. Gole, J. W. Stone, P. N. Sisco, A. M. Alkilany, E. C. Goldsmith and S. C. Baxter, *Acc. Chem. Res.*, 2008, **41**, 1721-1730.
6. J. Zhao, A. O. Pinchuk, J. M. McMahon, S. Li, L. K. Ausman, A. L. Atkinson and G. C. Schatz, *Acc. Chem. Res.*, 2008, **41**, 1710-1720.
7. F. J. García de Abajo, *Rev. Mod. Phys.*, 2007, **79**, 1267-1290.
8. S. Schlücker, *Angew. Chem. Int. Ed.*, 2014, **53**, 4756-4795.
9. R. A. Sperling, P. Rivera Gil, F. Zhang, M. Zanella and W. J. Parak, *Chem. Soc. Rev.*, 2008, **37**, 1896-1908.
10. L. Rivas, S. Sanchez-Cortes, J. V. García-Ramos and G. Morcillo, *Langmuir*, 2000, **16**, 9722-9728.
11. G. Guisbiers, R. Mendoza-Cruz, L. Bazán-Díaz, J. J. Velázquez-Salazar, R. Mendoza-Perez, J. A. Robledo-Torres, J.-L. Rodriguez-Lopez, J. M. Montejano-Carrizales, R. L. Whetten and M. José-Yacamán, *ACS Nano*, 2016, **10**, 188-198.
12. M. Fernanda Cardinal, B. Rodríguez-González, R. A. Alvarez-Puebla, J. Pérez-Juste and L. M. Liz-Marzán, *J. Phys. Chem. C*, 2010, **114**, 10417-10423.
13. D. Tsoutsi, J. M. Montenegro, F. Dommershausen, U. Koert, L. M. Liz-Marzán, W. J. Parak and R. A. Alvarez-Puebla, *ACS Nano*, 2011, **5**, 7539-7546.
14. H. Liao, A. Fisher and Z. J. Xu, *Small*, 2015, **11**, 3221-3246.
15. Y. Sun, B. T. Mayers and Y. Xia, *Nano Lett.*, 2002, **2**, 481-485.
16. Y. Sun and Y. Xia, *Science*, 2002, **298**, 2176-2179.
17. J.-F. Li, Y.-J. Zhang, S.-Y. Ding, R. Panneerselvam and Z.-Q. Tian, *Chem. Rev.*, 2017, **117**, 5002-5069.
18. J. Yang, J. Y. Lee and H.-P. Too, *J. Phys. Chem. B*, 2005, **109**, 19208-19212.
19. E. Roduner, *Chem. Soc. Rev.*, 2006, **35**, 583-592.
20. W. Ostwald, *Z. Phys. Chem.*, 1897, 289–330.
21. F. Liebig, A. F. Thünemann and J. Koetz, *Langmuir*, 2016, **32**, 10928-10935.
22. S. Abalde-Cela, S. Ho, B. Rodríguez-González, M. A. Correa-Duarte, R. A. Álvarez-Puebla, L. M. Liz-Marzán and N. A. Kotov, *Angew. Chem. Int. Ed.*, 2009, **48**, 5326-5329.
23. A. Mariño-López, M. Blanco-Formoso, L. N. Furini, A. Sousa-Castillo, E. Tiryaki, M. Pérez-Lorenzo, M. Testa-Anta, V. Salgueiriño, N. A. Kotov, R. A. Alvarez-Puebla and M. A. Correa-Duarte, *Langmuir*, 2019, **35**, 4110-4116.
24. N. G. Bastús, J. Comenge and V. Puntes, *Langmuir*, 2011, **27**, 11098-11105.
25. N. G. Bastús, F. Merkoçi, J. Piella and V. Puntes, *Chem. Mater.*, 2014, **26**, 2836-2846.
26. R. A. Alvarez-Puebla, E. Arceo, P. J. G. Goulet, J. J. Garrido and R. F. Aroca, *J. Phys. Chem. B*, 2005, **109**, 3787-3792.
27. N. Pazos-Perez, J. M. Fitzgerald, V. Giannini, L. Guerrini and R. A. Alvarez-Puebla, *Nanoscale Adv.* , 2019, **1**, 122-131.
28. A. S. Kumbhar, M. K. Kinnan and G. Chumanov, *J. Am. Chem. Soc.*, 2005, **127**, 12444-12445.
29. L. Litti and M. Meneghetti, *Phys. Chem. Chem. Phys.*, 2019, **21**, 15515-15522.
30. L. Rodríguez-Lorenzo, R. A. Álvarez-Puebla, I. Pastoriza-Santos, S. Mazzucco, O. Stéphan, M. Kociak, L. M. Liz-Marzán and F. J. García de Abajo, *J. Am. Chem. Soc.* , 2009, **131**, 4616-4618.
31. Z. Tang, N. A. Kotov and M. Giersig, *Science*, 2002, **297**, 237-240.
32. R. L. Penn and J. F. Banfield, *Science*, 1998, **281**, 969-971.
33. J. J. De Yoreo, P. U. P. A. Gilbert, N. A. J. M. Sommerdijk, R. L. Penn, S. Whitelam, D. Joester, H. Zhang, J. D. Rimer, A. Navrotsky, J. F. Banfield, A. F. Wallace, F. M. Michel, F. C. Meldrum, H. Cölfen and P. M. Dove, *Science*, 2015, **349**, aaa6760.
34. T. Kizuka, *Phys. Rev.Lett.*, 1998, **81**, 4448-4451.
35. Y. Lu, J. Y. Huang, C. Wang, S. Sun and J. Lou, *Nat. Nanotech.*, 2010, **5**, 218.
36. J.-Y. Kim, M.-G. Han, M.-B. Lien, S. Magonov, Y. Zhu, H. George, T. B. Norris and N. A. Kotov, *Sci. Adv.*, 2018, **4**, e1700682.
37. Y. Xia, T. D. Nguyen, M. Yang, B. Lee, A. Santos, P. Podsiadlo, Z. Tang, S. C. Glotzer and N. A. Kotov, *Nat. Nanotech.*, 2011, **6**, 580.
38. R. Holze, *Phys. Chem. Chem. Phys.*, 2015, **17**, 21364-21372.
39. E. B. Wilson, *Phys. Rev.*, 1934, **45**, 706-714.
40. R. Alvarez-Puebla, L. M. Liz-Marzán and F. J. García de Abajo, *J. Phys. Chem. Lett.*, 2010, **1**, 2428-2434.

41. D. M. Solís, J. M. Taboada, F. Obelleiro, L. M. Liz-Marzán and F. J. García de Abajo, *ACS Photonics*, 2017, **4**, 329-337.
42. P. Aldeanueva-Potel, E. Carbó-Argibay, N. Pazos-Pérez, S. Barbosa, I. Pastoriza-Santos, R. A. Alvarez-Puebla and L. M. Liz-Marzán, *ChemPhysChem*, 2012, **13**, 2561-2565.
43. M. Blanco-Formoso, A. Sousa-Castillo, X. Xiao, A. Mariño-Lopez, M. Turino, N. Pazos-Perez, V. Giannini, M. A. Correa-Duarte and R. A. Alvarez-Puebla, *Nanoscale*, 2019, **11**, 21872-21879.
44. D. Paramelle, A. Sadovoy, S. Gorelik, P. Free, J. Hobley and D. G. Fernig, *Analyst*, 2014, **139**, 4855-4861.
45. W. Stöber, A. Fink and E. Bohn, *J. Colloid Interface Sci.*, 1968, **26**, 62-69.
46. I. A. Ibrahim, A. Zikry and M. A. Sharaf, *J. Am. Sci*, 2010, **6**, 985-989.